Modeling of hygrothermal transfers through a bio-based multilayered wall tested in a bi-climatic room

Nicolas Reuge, Florence Collet, S. Pretot, Sophie Moissette, Marjorie Bart, C. Lanos

Authors contributions

N. Reuge, F. Collet, S. Pretot, S. Moissette, M. Bart, C. Lanos: Conceptualization, Methodology, Software, Validation, Formal analysis, Investigation, Resources, Writing – Original Draft, Writing – Review & Editing, Visualization

C. Lanos: Supervision, Project Administration

Modeling of hygrothermal transfers through a bio-based multilayered wall tested in a bi-climatic room

N. Reuge*, F. Collet, S. Pretot, S. Moissette, M. Bart, C. Lanos

Université de Rennes, Laboratoire de Génie Civil et Génie Mécanique, Axe Ecomatériaux pour la construction, 3 rue du Clos Courtel, BP 90422, 35704 Rennes, France

*Corresponding author, reuge@free.fr – phone: +33 6 01 90 15 78, ORCID: 0000-0003-4764-990X

Abstract

A bio-based multilayered wall has been developed in the framework of the European ISOBIO project. A key point was to be able to perform proper simulations of the hygrothermal transfers occurring through the wall: local predictions are of first importance to characterize the behavior of the wall and thereafter its ability to ensure comfortable hygrothermal conditions inside buildings. A previous study proved that the conventional assumption of an instantaneous equilibrium between local relative humidity and water content according to the sorption isotherm is not relevant for bio-based porous materials, where in practice slow sorption kinetics occur. In the present study, an improved expression of the local kinetics is proposed and validated by sorption experiments. Then, Moisture Buffer Value tests are performed (Nordtest project's protocol). The simulations are adjusted to these measurements by using the inverse method in order to refine the knowledge of some critical parameters. Depending on the studied materials, the local kinetics constants are between 0.15 and 14 $day^{-1}/(kg.m^{-3})$. Finally, the ISOBIO wall is studied in a bi-climate room under a wide range of operating conditions. Simulations carried out with the conventional approach (TMC) and the local kinetics approach (TMCKIN) are compared to measurements: this clearly shows that the latter is able to predict well the relative humidity dynamics while the former underestimates it by a factor up to 66%. These results highlight the relevance of the new expression of the local kinetics and its ability to describe well the local hygric dynamics is certainly an achievement.

Keywords

Bio-based building materials; Local kinetics; Sorption; Moisture buffering; Hygrothermal transfer; Modeling

1 Introduction

In the framework of the European ISOBIO project (featuring the slogan "naturally high-performance insulation"), a multilayered wall made of bio-based materials involving very low carbon footprints and high insulating properties has been developed. One of the key points of this project was to be able to perform reliable simulations of the hygrothermal transfers occurring inside this ISOBIO reference wall. The main difficulty with such simulations is to correctly describe hygric phenomena in bio-based materials. Reuge et al. work on this subject and several studies are already available [1, 2].

Besides their good insulating properties, bio-based materials are usually excellent moisture regulators [3, 4]. In their experimental and modeling study, Mnasri et al. [5] demonstrated the potential of bio-based materials (and more particularly a wood-cement composite) to improve hygrothermal comfort and buildings energy consumption.

Water sorption in porous media involves various phenomena: the transport is ruled by vapor / liquid water diffusion and the water sorption by the equilibrium isotherms of adsorption / desorption coupled with hysteretic phenomena. The diffusivities can be measured by permeability tests (*i.e.* "wet cup method" [6]). The main equilibrium isotherms of sorption also known as "water storage functions" can be measured by gravimetric methods [7]. The actual water content evolves between the main adsorption and desorption isotherms as a function of the relative humidity along hysteretic paths as described by some rather complex models such as the Carmeliet model [8] and the Huang model [9]. They consider local memory effects depending on the full hygroscopic history of the studied materials.

However, the aforementioned models are not sufficient to provide a good description of the hygric state in these porous media. Actually, conventional simulations greatly underestimate the time required for the water content to reach the equilibrium. This was shown for bio-based materials: in [10] for cellulosic materials, in [11] and [12] for wood, in [13] for paperboard, by Reuge et al. in [1] and [2] for ISOBIO materials and in [14] and [15] for various hemp-lime concretes, but also for more classic compounds such as cements [16, 17]. These deviations obtained from conventional models are of particular concern when hygric transfers are subject to permanent fluctuations of relative humidity (*RH*) such as in building envelope materials, food materials or soils. Several expressions for the local kinetics of sorption can be found in the aforementioned references. A kinetics is usually expressed as a kinetic constant multiplied by a driving force. In most of the aforementioned studies, the authors have proposed to express the driving force as a function of local relative humidities with more or less success. The problem is that they consider an equilibrium relative humidity which is a priori not known for a local approach and / or they have to change the value of the kinetics constant according the operating conditions. Actually, it seems more natural to express the driving force as a function of the local water content, as done by Nyman et al. [10] and Johannesson and Nyman [16]. This will be detailed in section 4.1.

Thus, conventional approaches describing hygrothermal transfers in building materials are based on the assumption that for a given local relative humidity φ, the corresponding equilibrium local water content w is reached instantaneously (Künzel approach [18]). In our previous studies [1, 2, 14, 15], various bio-based materials were studied and it was demonstrated that such an assumption led to patent inconsistencies such as a water vapor / liquid water equilibrium reached too fast at the local scale and at the sample scale and / or underestimation of the local *RH* dynamics. Thus, as reported in the aforementioned literature, our previous studies have established that a local kinetics of sorption exists (from water vapor to liquid water and inversely) which can be slow compared to the diffusive phenomena.

In this study, an improved expression of the local kinetics of sorption is proposed and validated by experimental results allowing to obtain better results from the simulations for small time scales (from seconds to a few hours).

To our knowledge, this is the first modeling work studying a fully bio-based multilayered wall in the controlled conditions of a bi-climatic room while various studies have already been carried out considering only one bio-based layer. Moujalled et al. [19] have studied the effect of real climatic conditions (Périgueux, FR) on a bio-based building with a wall of three layers: a hemp-lime concrete but with classic internal and external renders. Their results of the simulations were broadly in good agreements with the measurements but the small time scale (on a few hours) *RH* dynamics was very notably underestimated. Piot et al. [20] have also studied a three-layered wall (Savoie, FR) in real climatic conditions: a hemp concrete wall but also with classic internal and external renders. Again, the calculated small time scale *RH* dynamics was very notably underestimated compared to the

measurements. In the studies of Lelievre et al. [21], Colinart et al. [22, 23], Rahim et al. [24], Fabbri and McGregor [25] and Seng and al. [26], the authors have studied the response of hemp concrete panels to controlled indoor and outdoor conditions. Even in these controlled operating conditions, most of these studies led to simulation results that underestimate clearly the small time scale *RH* dynamics. From that point of view, some studies seem to obtain better results playing on the temperature dependence of the sorption isotherms [23, 24] or on the slope of the sorption curve [25] or on some parameters which have an effect on the hysteretic behavior of the sorption phenomena such as the initial water content (which is usually unknown) and / or on the considered hysteretic model [21].

The first part of this study is a summary of the classic hygric and thermal properties measured on samples of ISOBIO wall materials. Some classic models are used and adjusted to describe these properties evolutions as a function of water content or relative humidity. Then, the governing equations describing the hygrothermal transfers are given. In the following part, the expression of the sorption rate previously defined is recalled and a fine modeling of the global kinetics of the sorption measurements is used to define the improved expression of the sorption rate. This allows better predictions at the beginning of the sorption process. Then, MBV tests are simulated and adjusted to measurements by the inverse method: these adjustments allow refining the knowledge of some critical parameters. Finally, a hygrothermal study is performed at the wall scale. Experiments are carried out on the ISOBIO test wall under controlled climatic conditions of a bi-climatic room. This provides experimental data to be compared to the simulations based on the classical approach and to the simulations carried out with the new kinetic model, these two approaches leading to different predictions of the local relative humidity dynamics.

2 ISOBIO materials and hygrothermal properties

2.1 Reference ISOBIO wall

The reference ISOBIO wall is made of the layering of several materials / panels: a BCB^{TM} lime-hemp render (BCB), a CAVAC^{TM} Rigid insulation panel made of hemp shiv and an organic binder (CAV), a Biofib Trio flexible insulation panel from CAVAC^{TM} made of hemp flax and cotton (BIO1), an OSB3 panel, a Proclima^{TM} INTELLO membrane (INT), a second Biofib Trio flexible insulation panel (BIO2), a Lignicell CSB^{TM} panel made of compressed straw (CSB) and a CLAYTEC^{TM} clay-hemp plaster (CLA). Note although a timber frame supports this wall, this will be ignored in the simulations. This ISOBIO reference wall and the layers thicknesses are shown in Figure 1.

Figure 1

2.2 Hygrothermal properties

This section summarizes the values of the properties needed to perform the simulations, *i.e*. the materials densities ρ_0, porosities ε_0, vapor diffusion resistance factors μ_0, thermal conductivities λ_0 and specific heat capacities Cp_0: they are reported in Table 1. While most of them come from [27] where experimental methods and measurement are provided, a few others come from trustable technical sheets.

The isotherms of adsorption of representative samples of ISOBIO materials (CAV, BIO, OSB3 and CSB) have been determined in [27]. The moisture storage functions of the other ISOBIO materials come from technical sheets and / or Fraunhofer Institute for Building Physics (F-IBP) databases (BCB, INT and CLA).

Table 1: ISOBIO materials properties at dry state at T = 23°C with margins of error

	ρ_0 ±5% (kg.m^{-3})	ε_0 ±5% (-)	μ_0 ±10% (-)	λ_0 ±5% (W.m^{-1}.K^{-1})	Cp_0 ±10% (J.kg^{-1}.K^{-1})
BCB	530	0.546	9	0.13	1006
CAV	190	0.874	11	0.07	2100
BIO	26.5	0.98	3.6	0.039	1800
OSB3	551	0.609	138	0.13	1600
INT	85	0.085	$1.364.10^5$	2.4	2500
CSB	449	0.72	27	0.10	1700
CLA	1392	0.294	10	0.62	1040

2.3 Models of properties

The appropriate models of properties needed for the simulations have been studied in [2]. For the isotherms of adsorption, the Van Genuchten model (VG) [28] has been used. It is claimed valid even near the liquid water saturation state and is expressed as follow:

$$W_{eq}\left(RH\right)=W_{sat}\left[1+\left(-h\ln\left(RH\right)\right)^{\eta}\right]^{1-1/\eta} \tag{1}$$

where W_{eq} is the sample water content at equilibrium, W_{sat} is the maximum water content in the sample, h and η are adjustment coefficients. The values of these adjustment coefficients are given in Table 2 and the experimental and modeled isotherms of adsorption of CAV and CSB are shown in Figure 2.

Figure 2

The hygric dependence of the vapor diffusion resistance factors μ has been neglected except for the Proclima INTELLO because this is a hygrovariable membrane evolving very significantly as a function of the moisture content (from 550 at 100% RH to 136400 at 0% RH). The data provided by Proclima / F-IBP have been fitted by a logistic power law [1, 2] (because of its great values, this parameter must be carefully modeled): $\mu=1/\left(a+b.RH^{c}\right)$, with: a = 7.3310^{-6}, b = 1.8.10^{-3} and c = 7.644.

Finally, the hygric dependence of the thermal conductivities has been described by the self-consistent scheme [29], which takes the following expression:

$$\begin{aligned}\lambda\left(W\right)=\lambda_s\Big\{1+\varepsilon_0\Big[\left(1-\varepsilon_0\right)/3+\left(3+\left(W/1000\varepsilon_0\right)\left(\lambda_a/\lambda_w-1\right)\right)\\ \cdot\left(3\left(\lambda_a/\lambda_s-1\right)-\left(W/1000\varepsilon_0\right)\left(\lambda_a/\lambda_w-1\right)\left(2\lambda_w/\left(\lambda_s+1\right)\right)\right)^{-1}\Big]^{-1}\Big\}\end{aligned} \tag{2}$$

where λ_a (0.025 W.m^{-1}.K^{-1}) is the air thermal conductivity and λ_w (0.6 W.m^{-1}.K^{-1}) is the liquid water thermal conductivity. The coefficient λ_s has been adjusted such as $\lambda(W$=0) equals λ_0. The values of λ_s are given in Table 2.

Note that the expressions (1) and (2) are written at the sample scale but they remain valid at the local scale replacing RH by the local relative humidity φ and W by the local water content w.

Table 2: Adjustment coefficients for the VG model (h and η) and the self-consistent scheme (λ_s)

	W_{sat} (kg.m^{-3})	h (-)	η (-)	λ_s (W.m^{-1}.K^{-1})
BCB	546	8524	1.38	0.312
CAV	874	27490	1.435	0.53
BIO	348	228504	1.473	1.055
OSB3	609	11360	1.325	0.367
INT	85	2091	1.42	2.74
CSB	720	23172	1.334	0.38
CLA	294	271	1.656	0.995

3 Mathematical modeling

3.1 Mass transport governing equations

As classically assumed, (*i*) air transport is ignored. In the porous materials, water is present as water vapor and liquid. Thus, two mass balance equations have to be considered. Assuming that (*ii*) the convective transport is negligible, they are given by (*cf.* [1, 2, 15]):

$$\begin{cases} \dfrac{\partial\left(\varphi P_{sat}\right)}{\partial t} - \nabla\cdot\left[\delta_{v,p}\dfrac{RT}{M_w}\nabla\left(\varphi P_{sat}\right)\right] = -\dfrac{RT}{M_w}R_s \\ \dfrac{\partial w}{\partial t} - \nabla\cdot\left(D_{p,l}\nabla w\right) = R_s \end{cases} \tag{3,4}$$

where the porous media vapor permeability is given by: $\delta_{v,p} = \delta_v/\mu = D_v M_w/\mu RT$ and the water vapor diffusion resistance factor by: $\mu = \delta_v/\delta_{v,p} = D_v/D_{p,v}$, $D_{p,v}$ and $D_{p,l}$ being the water vapor and liquid water diffusivities in the porous media respectively.

The sorption rate R_s will be detailed in section 4. It is commonly assumed that R_s is very fast compared to the vapor diffusive flux. This is not the case for the bio-based materials studied here. Note that according to this common assumption, the following single governing equation can be obtained:

$$\left.\frac{\partial w}{\partial\varphi}\right|_T \frac{\partial\varphi}{\partial t} - \nabla\cdot\left[\left(\delta_{v,p}P_{sat} + D_{p,l}\left.\frac{\partial w}{\partial\varphi}\right|_T\right)\nabla\varphi\right] = 0 \tag{5}$$

Equation (5) is the so-called Künzel mass transfer equation [18].

The classic heat transport governing equation is not given here but it is obviously taken into account considering latent heat of vaporization.

3.2 Boundary conditions

At the wall or sample edge edg_i, the local relative humidity is given by:

$$\varphi_{edg_i} = RH - \frac{\delta_{v,p}}{h_m} \cdot \nabla\varphi\big|_{edg_i} \tag{6}$$

where h_m is the mass transfer coefficient. The local water content gradient is given by:

$$\nabla w\big|_{edg_i} = \beta \left.\frac{\partial w}{\partial \varphi}\right|_T \nabla\varphi\big|_{edg_i} \tag{7}$$

where β is in the range of 0 to 1 and dynamically depends on the sorption rate R_s. Its value will be considered as a constant value of 1. It was shown in [1, 15] that its value (0 or 1) does not impact the simulation results.

4 Improvement and validation of the local kinetic model of sorption

4.1 State of the art

In their studies, Nyman et al. [10] and Johannesson and Nyman [16] have proposed the following expression for the sorption rate:

$$R_s = k_0 \left(w_{eq}(\varphi) - w \right) \tag{8}$$

where k_0 is the local kinetic constant of sorption (adsorption or desorption) and w_{eq} is the equilibrium local water content given by the sorption isotherm at a local relative humidity φ.

Independently, our very first investigations have led to establish the same expression. However, the value of the kinetic constant k_0 still has to be adjusted as a function of the operating conditions: this was not really satisfactory, the local kinetic constant should only depend on the porous materials and not on the hygric conditions, at least as long as the hygric state is far from saturation.

From Reuge et al. [14, 15], the sorption rate R_s is preferably expressed as follow:

$$R_s = \pm k_0 \left(w_{eq}(\varphi) - w \right)^2 \tag{9}$$

where k_0 (day^{-1}/(kg.m^{-3})) is a kinetic constant of a second order kinetics. The sign in front of k_0 is the same as the sign of $\left(w_{eq}(\varphi) - w \right)$, *i.e.* plus for adsorption, minus for desorption. Using this second order local kinetics, k_0 can be kept constant for a wide range of *RH*, at least between 30% and 70% *RH* [14, 15].

4.2 Sorption experiments and improvement of the sorption rate expression

Figure 3 shows the kinetics of water adsorption of a CAV sample [27]. The sample had been initially stabilized at a given *RH* and suddenly submitted to a greater ambient *RH* (0-30% *RH*, 30-50% *RH* and 50-65% *RH*). For the 0-30% *RH* and 50-65% *RH* steps, the sample has been weighted continuously whereas for the 30-50% *RH* step, only discontinuously values are available due to a computer failure. In Fig. 3, the measurements and the results of the simulations of these tests are compared. As an illustration, a simulation has been carried out using the Künzel approach for the 30-50% *RH* step: the stabilization is predicted after two days while it takes weeks according to the measurements (Fig. 3). Then, simulations have been carried out using expression (9) for the sorption rate with the kinetic constant k_0 as adjustment parameter. Broadly, the adjustments are good but if the comparison is focused at the very beginning of the process, it appears that the adjustments are not so good, this is

particularly noticeable within the first day: the simulations tend to underpredict the adsorption rate. Thus, the following new expression is proposed for the sorption rate:

$$R_s = \left(\pm k_{01} + k_{02} \frac{\partial \varphi}{\partial t} \right) \left(w_{eq}(\varphi) - w \right)^2 \quad (10)$$

where k_{01} (day^{-1}/(kg.m^{-3})) and k_{02} (m^3.kg^{-1}) are kinetic constants.

While the term $k_{01}\left(w_{eq}(\varphi) - w \right)^2$ describes the slow diffusion of bound water molecules in the biological cells as explained in [15], the new term $k_{02}\frac{\partial \varphi}{\partial t}$ would describe the sudden capillary sorption of water in the macropores due to the Kelvin effect [30] occurring immediately during a sudden variation of local relative humidity φ. This new expression has the advantage to complexify the previous expression of the sorption rate (9) without denaturing its physical sense, sorption remains driven by $\left(w_{eq}(\varphi) - w \right)$ and expression (10) tends towards expression (9) in the absence of stiff variation of φ.

As shown in Figure 3, very good adjustments are obtained using k_{01} equal to $0.75k_0$ (k_0 = 0.56 day^{-1}/(kg.m^{-3}) for 0-30% *RH* step and k_0 = 0.3 day^{-1}/(kg.m^{-3}) for 30-50% *RH* and 50-65% *RH* steps) and values of k_{02} equal to $0.5.10^5$ m^3.kg^{-1} for the 0-30% *RH* step and 3.10^5 m^3.kg^{-1} for the 30-50% *RH* and 50-65% *RH* steps. Considering the first two days of the 0-30% *RH* step, the correlations coefficients *r* between the measurements and the simulations carried out using the kinetics model (9) and (10) are of 0.997 and 0.999 respectively. Considering the first two days of the 50-65% *RH* step, the correlations coefficients *r* between the measurements and the simulations carried out using the kinetics model (9) and (10) are of 0.994 and 0.999 respectively. They are clearly in favor of the kinetics model (10).

For standard operating conditions (*RH* > 30%), the following expression of the sorption rate can be deduced:

$$R_s = k_0 \left(\pm 0.75 + 10^6 \frac{\partial \varphi}{\partial t} \right) \left(w_{eq}(\varphi) - w \right)^2 \quad (11)$$

There is no guarantee that this expression is valid whatever the bio-based material but it will be assumed to be so. However, note that this expression allows to carry out sorption simulations that are in agreement with the measurements for all the studied ISOBIO materials and also for the hemp concretes studied in [15].

From [2], the values of the kinetic constant k_0 are given in Table 3. Its values for OSB3, INT and CLA remain unknown.

Figure 3

Table 3: ISOBIO materials kinetic constants k_0 obtained by adjusting simulations to sorption measurements [2]

	k_0 (day^{-1}/(kg.m^{-3}))
BCB	0.005
CAV	0.3
BIO	14
CSB	0.25

5 MBV tests: measurements and simulations

5.1 Measurements

Representative samples of ISOBIO materials have been subject to standard Moisture Buffer Value (MBV) tests according to the Nordtest project's protocol [27]. It relates the amount of moisture uptake / release to the exchange area and to the relative humidity step during daily cyclic variations (8 hours at ≈75% *RH*, and 16 hours at ≈33% *RH*). The recorded ambient *RH* is shown in Figure 4 (smoothed curve). Note that the last cycle is uncomplete due to technical issues.

Figure 4

The obtained MBV values have been reported in [27], they are of 1.7, 0.77, 1 and 0.53 g/(m².%*RH*) for CAV, CSB, BCB and OSB3 respectively. For the present study, it is interesting to consider the temporal evolution of the relative water mass Δm_w of the samples during the tests. The results of these measurements are presented in Figures 5 (CAV), 6 (CSB), 7 (BCB) and 8 (OSB3).

5.2 Simulations

Then, simulations have been carried out with home-made 1D Cartesian tools, TMC based on the Künzel approach (5) and TMCKIN based on the kinetics approach (3, 4, 11). Initially, the samples had been stabilized at 50% *RH* at a temperature of 22.6°C, these initial conditions have been used for the simulations. The mass transfer coefficient h_m at the exposed samples surface has been considered equal to 4.10^{-8} kg.m^{-2}.Pa^{-1}.s^{-1} [31, 32].

The right amplitudes of the *W* variations have been obtained by adjusting the water vapor diffusion resistance factor μ to a value between μ_0 (25% *RH*) and the lower μ_{humid} (70.5% *RH*, see [27]) for each material: this is consistent with the actual water content of the materials.

As shown in Figures 5 (CAV) and 6 (CSB), the results of the simulations are in good agreements with the measurements but the results obtained with TMCKIN appear significantly better than those obtained with TMC. The simulations named "TMC bis" are carried out with TMC using the values of μ obtained from the adjustments of TMCKIN simulations. Note that with TMC, the adjustment for CSB was not possible with μ between μ_{humid} and μ_0, a greater value than μ_0 had to be considered.

Figure 5

Figure 6

Figure 7

Figure 8

Regarding BCB (Fig. 7), results are not good at all with TMC, no adjustment could be done since μ_0 and μ_{humid} have the same value of 9 (from measurements performed at University of Bath) ; in order to obtain a decent adjustment with TMCKIN, a value of k_0 of 0.15 day^{-1}/(kg.m^{-3}) has to be considered instead of the previous value of 0.005 day^{-1}/(kg.m^{-3}) given in Table 3: this is not surprising since the data used in [2] to determine this kinetic constant were not appropriate (*i.e*. desorptions from 100% *RH*, far beyond the common range of *RH*).

Finally, as shown in Figure 8 for OSB3, the adjustment with TMCKIN has allowed to determine a value of k_0 for this material, which is 0.4 day^{-1}/(kg.m^{-3}).

According to these results, some values of k_0 can be updated as shown in Table 4. The values of μ used for the adjustments and the correlation coefficients between measurements and simulations are also reported in this table. Note that the correlations coefficients are not always better with TMCKIN than with TMC: this is due to the fact that the adjustments have been carried out considering the minimum and maximum points of the measurements whereas the correlation coefficients have been calculated with respect to all the experimental points.

Table 4: ISOBIO materials kinetic constants k_0 updated, values of μ obtained from adjustments of TMC and TMCKIN on MBV tests and correlation coefficients *r*

	k_0 ($day^{-1}/(kg.m^{-3})$)	μ (TMC)	*r* (TMC)	μ (TMCKIN)	*r* (TMCKIN)
BCB	**0.15**	9	0.479	9	0.981
CAV	0.3	6.75	0.995	5.5	0.997
BIO	14	-	-	-	-
OSB3	**0.4**	100	0.995	80	0.989
CSB	0.25	40	0.995	27	0.992

Note that the adjusted values of μ are lower with TMCKIN than with TMC (and then closer to μ_{humid}). It is also important to note that some tries have been carried out using the old expression (9) of the kinetics model but it was quite impossible to obtain as good adjustments as with the new expression (11): the amplitudes of the *W* variations were systematically underestimated; The only solution to obtain descent adjustments with (9) was to consider greater k_0, typically by one order a magnitude: this is obviously not satisfactory and support the relevancy of the model (11).

For the CAV material, Figure 9 shows full hygric cycles (w, φ) obtained with TMC and TMCKIN between t = 48 h and t = 72 h at 2 mm and 2 cm depths. According to the TMC simulation results, (w, φ) logically moves along the adsorption isotherm whereas the TMCKIN simulation leads to (w, φ) moving around this adsorption isotherm.

Still for the CAV material, Figure 10 shows the water content profiles and the relative water content distributions referring to the initial water content W_{eq}(50% *RH*) as a function of sample depth at t = 48 h and t = 56 h obtained with (a) TMC and (b) TMCKIN. Regarding the water content distributions, mean values corresponding to slices of 1 cm depth are estimated integrating the calculated local water contents.

Note that the MBV measurements [27] have been carried out on a 5 cm deepness sample of this material, *i.e*. exactly the deepness of the CAV panel in the ISOBIO reference wall.

Figure 9

Figure 10

The water content variations predicted by TMC between 3 cm and 4 cm (Fig. 10a) and by TMCKIN between 4 cm and 5 cm (Fig. 10b) are so low that the MBV values are very slightly affected by these slices; Thus, the penetration depth is slightly greater according to TMCKIN simulation than according to TMC simulation. From TMC and TMCKIN simulations, minimum sample depths of 4 cm and 5 cm are respectively required to ensure a very reliable MBV determination for the CAV sample.

6 Study of the ISOBIO wall in a bi-climatic room

6.1 Experimental setup

The ISOBIO reference wall has been studied in the controlled environments of a bi-climatic room (Figure 11). The walls of the bi-climatic room are made of rigid insulation panels covered with steel sheets and the floor is a concrete slab, meaning the humidity or thermal exchanges between indoor and outdoor remain low. The ISOBIO wall (surface of about 1.2 m^2) acted as separation between the two climatic rooms. Temperature and relative humidity have been measured thanks to 41 sensors (SHT35 Sensirion sensors) placed at different depths inside the wall and additional sensors were placed on the wall surfaces and in ambient environments.

6.2 Operating conditions

The measurements performed can be divided in three main period, 1, 2 and 3. The boundary conditions applied (*i.e*. *T* and *RH* at the wall surfaces) are shown in Figures 12a&b, 12c&d, 12e&f for the periods 1 (1128 h), 2 (340 h) and 3 (148 h) respectively. The room contiguous to the BCB render is called "outdoor" while the room contiguous with the CLA plaster is called "indoor".

Initially, before period 1, the wall has been stabilized at 50% *RH*, 23°C but some chamber regulation tests performed just before period 1 may have result in a loss of the wall stabilization. During period 1, some monitoring issues had occurred around a time of 400 h, during this interval, *RH* and *T* setpoints are considered as boundary conditions (*i.e*. flat part). Period 2 is consecutive to period 1. Period 3 is not consecutive to period 2 but the wall has been stabilized again at 50% *RH*, 23°C before this last period.

Figure 11

6.3 Comparison of measurements and simulations

6.3.1 Assumptions

Simulations have been carried out with TMC and TMCKIN, assumptions are given in sections 3 and 4. Regarding TMCKIN simulations, expression (11) of the sorption rate have been considered. ISOBIO materials kinetic constants k_0 given in Table 4 have been used. For INT and CLA layers, the associated k_0 are unknown but a median value of 0.25 $day^{-1}/(kg.m^{-3})$ has been considered. No hysteric effect has been considered for the sorption mechanism. For the materials BCB, CAV, OSB3 and CSB, the values of μ obtained from the adjustments (TMC & TMCKIN) in the previous section (Table 4) have been considered. For BIO and CLA, μ_0 has been considered (*cf*. Table 1). For INT, the logistic power law of μ has been used (*cf*. section 1).

At the beginning of period 1 and period 3, the wall is assumed stabilized at 50% *RH*, 23°C. The initial conditions of period 2 are the final conditions of period 1. Lastly, *RH* and *T* have been measured at the wall surfaces (Fig. 12) and therefore are considered as Dirichlet boundary conditions for the simulations.

6.3.2 Results and discussion

The results (measurements and simulations) are analyzed at these positions equipped with (*RH*-*T*) sensors:

- position 1, CAV / BIO1 interface (8 cm depth),

- position 2, BIO1 / OSB3 interface (22.5 cm depth),

- and position 3, INT / BIO2 interface (23.75 cm depth).

As shown in Figure 13a, temporal evolutions of *RH* obtained by TMCKIN fit more closely the measurements than those obtained by TMC, at position 1 during period 1. At positions 2 and 3 (Fig 13b and 13c), TMC and TMCKIN simulations are very close but underpredict *RH* (by 5% at most) likely due to inadequate initial conditions: technical issues have indeed disturbed the hygric stabilization prior to period 1 resulting in somewhat imperfect knowledge of initial hygric state and hygric history of the wall and then in the simulations offsets. In Figure 13b, TMC simulation underestimates the *RH* fluctuation by 18.5% while TMCKIN simulation underestimates it by only 11%.

As shown in Figure 14a, *i.e*. at position 1 during period 2, TMC simulation underpredicts the amplitude of the *RH* variations by 30% whereas TMCKIN results overpredict them by 40%. A position 2 (Fig. 14b), TMC simulation largely underpredicts the *RH* variations by 66%, TMCKIN simulation is much closer to the measurements even if it still underpredicts the *RH* variations by 12%. At position 3 (Fig. 14c), TMCKIN simulation still leads to better results than TMC predicting exactly the amplitude of the *RH* variations. Overall, discrepancies that still persists between TMCKIN simulation and measurements can be imputed to not taking into account the hysteretic phenomena (note that this would demand a perfect knowledge of the whole hygric history of the wall).

As shown in Figure 15a and 15b, *i.e*. at position 1 & 2 during period 3, TMCKIN simulation better predicts the *RH* variations than TMC simulation. At position 2, this is more clearly illustrated in Figure 16 where the TMC & TMCKIN *RH* curves has been raised by a value of +2%*RH* to compensate the offsets: the correlation coefficients between measurements / TMC simulation and measurements / TMCKIN simulation are of 0.824 and 0.896 respectively. In other words, with TMCKIN, the *RH* dynamics is better predicted. This is obviously an effect of the sorption kinetics model. Note that the temperatures evolutions predicted by the simulations are not presented here but they are in perfect accordance with the measurements.

Figure 12

Figure 13

Figure 14

Figure 15

Figure 16

Finally, TMCKIN simulations are overall in significantly better agreement with the measurements than TMC simulations. It clearly shows the benefit of using the sorption kinetics model (11) on the *RH* dynamics prediction.

7 Conclusions

The huge campaign of characterization and testing of the ISOBIO materials has allowed to carry out hygrothermal transfers simulations.

It has been shown that the expression of the local sorption rate used in previous studies could be improved to better describe the early beginning of the sorption process. The global sorption

measurements performed at the scale of a large sample have allowed to validate the new expression of this model: this is the first step forward brought by this study.

Then, the simulations carried out with TMC (based on Künzel approach) and TMCKIN (based on the kinetics of sorption model) have been adjusted on some Moisture Buffer Value measurements. The results obtained with TMCKIN are in good agreement with measurements. It is worth noting that TMCKIN predicts slightly deeper moisture penetration depths than TMC. These results can be of some interest to guide the experimenters in performing Moisture Buffer Value measurements: this is the second step forward brought by this study.

Finally, the ISOBIO reference wall has been studied in a bi-climatic room with in-situ *RH* measurements: this is an unprecedented experimental work for a multilayered fully bio-based wall. This wall was submitted to various hygrothermal conditions. Simulations have been carried out and compared to the measurements. It has been shown that TMCKIN led to better results than TMC predicting more realistic relative humidity dynamics. It shows the pertinence of the new sorption kinetics model, this is an achievement in the considered field. The underestimation of the relative humidity dynamics by the conventional model would lead to erroneous prediction of hygric conditions inside rooms for future whole building simulations, this is why the new approach presented in this study should be considered.

Future investigations possibly lead to even better results trying to take into account the hygric history of the wall more precisely.

Acknowledgments

This work has been performed and funded in the framework of the European project ISOBIO – (http://isobioproject.com) within the scope the of the research and innovation program Horizon 2020 (agreement No. 636835). This work has also been supported by the French region Bretagne Loire (UBL).

References

[1] N. Reuge, F. Collet, S. Moissette, M. Bart, S. Pretot, C. Lanos, A local kinetics of sorption model: theoretical background and application to the simulation of an ISOBIO demonstrator, in: 3rd International Conference on Bio-Based Building Materials, Belfast, UK, June 26th – 28th 2019. https://doi.org/10.26168/icbbm2019.51.

[2] N. Reuge, F. Collet, S. Pretot, S. Moissette, M. Bart, O. Style, A. Shea, C. Lanos, Hygrothermal effects and moisture kinetics in a bio-based multi-layered wall: Experimental and numerical studies, Constr. Build. Mater. 240 (2020) available online. https://doi.org/10.1016/j.conbuildmat.2019.117928.

[3] O. Douzane, G. Promis, J.-M. Roucoult, A.-D. Tran Le, T. Langlet, Hygrothermal performance of a straw bale building: In situ and laboratory investigations, J. Build. Eng. 8 (2016) 91-98. https://doi.org/10.1016/j.jobe.2016.10.002.

[4] U. Dhakal, U. Berardi, M. Gorgolewski, R. Richman, Hygrothermal performance of hempcrete for Ontario (Canada) buildings, J. Clean. Prod. 142 (2017) 3655-3664. https://doi.org/10.1016/j.jclepro.2016.10.102.

[5] F. Mnasri, S. Bahria, M. E.-A. Slimani, O. Lahoucine, M. El Ganaoui, Building incorporated bio-based materials: Experimental and numerical study, J. Build. Eng. 28 (2020) available online. https://doi.org/10.1016/j.jobe.2019.101088.

[6] M. Kumaran, Interlaboratory Comparison of the ASTM Standard Test Methods for Water Vapor Transmission of Materials (E 96-95), J. Test. Eval. 26(2) (1998) 83–88. https://doi.org/10.1520/JTE11977J.

[7] H.A. Iglesias, J. Chirife, Handbook of Food Isotherms: Water Sorption Parameters for Food and Food Components, Academic Press Inc., United Kingdom Edition, 1982. eBook ISBN: 9780323154277.

[8] J. Carmeliet, M. De Wit, H. Janssen, Hysteresis and moisture buffering of wood, in: 7th Nordic Symposium on Building Physics, Reykjavik, Islande, 2005. http://www.rabygg.is/bfys2005.

[9] H.C. Huang, Y.C. Tan, C.W. Liu, C.H. Chen, A novel hysteresis model in unsaturated soil, Hydrol. Process. 19(8) (2005) 1653-1665. https://doi.org/10.1002/hyp.5594.

[10] U. Nyman, P.J. Gustafsson, B. Johannesson, R. Hägglund, A numerical method for the evaluation of non-linear transient moisture flow in cellulosic materials, Int. J. Numer. Meth. Engng 66 (2006) 1859–1883. https://doi.org/10.1002/nme.1597.

[11] H.L. Frandsen, L. Damkilde, S. Svensson, A revised multi-Fickian moisture transport model to describe non-Fickian effects in wood, Holzforschung, Vol. 61(5), Copyright by Walter de Gruyter, Berlin, New York, pp. 563–572, 2007. ISSN 0018-3830.

[12] J. Eitelberger, S. Svensson, The sorption behavior of wood studied by means of an improved cup method, Transp. Porous Med. 92 (2012) 321–335. https://doi.org/10.1007/s11242-011-9905-8.

[13] M. Alexandersson, H. Askfelt, M. Ristinmaa, Triphasic model of heat and moisture transport with internal mass exchange in paperboard, Transp. Porous Med. 112 (2016) 381–408. https://doi.org/10.1007/s11242-016-0651-9.

[14] N. Reuge, S. Moissette, M. Bart, F. Collet, C. Lanos, Modèle de cinétique locale de sorption couplé au phénomène d'hystérésis pour les matériaux biosourcés, in : RUGC 2018, 36ème Rencontres Universitaires de Génie Civil de l'AUGC, Saint Etienne, France, June 20th-22nd 2018. https://doi.org/10.26168/ajce.36.1.11.

[15] N. Reuge, S. Moissette, M. Bart, F. Collet, C. Lanos, Water transport in bio-based porous materials: A model of local kinetics of sorption—Application to tree hemp concretes, Transp. Porous Med. 128(2) (2019) 821-836. https://doi.org/10.1007/978-981-15-0802-8_77.

[16] B. Johannesson, U. Nyman, A numerical approach for non-linear moisture flow in porous materials with account to sorption hysteresis, Transp. Porous Med. 84 (2010) 735–754. https://doi.org/10.1007/s11242-010-9538-3.

[17] H. Janssen, G. Albrecht Scheffler, R. Plagge, Experimental study of dynamic effects in moisture transfer in building materials, Int. J. Heat Mass Transf. 98 (2016) 141-149. https://doi.org/10.1016/j.ijheatmasstransfer.2016.03.031.

[18] H.M. Künzel, Simultaneous Heat and Moisture Transport in Building Components – One- and Two-Dimensional Calculation Using Simple Parameters, Fraunhofer IRB Verlag Suttgart, ISBN 3-8167-4103-7, 1995. https://doi.org/ISBN v.3-8167-4103-7.

[19] B. Moujalled, Y.A. Ouméziane, S. Moissette, M. Bart, C. Lanos, D. Samri, Experimental and numerical evaluation of the hygrothermal performance of a hemp lime concrete building: A long term case study, Build. Environ. 136 (2018) 11–27. https://doi.org/10.1016/j.buildenv.2018.03.025.

[20] A. Piot, T. Béjat, L. Bessette, A. Jay, Hygrothermal behaviour of a hemp concrete wall: experimental and numerical study of coating, in: First International Conference on Bio-based Building Materials, Clermont-Ferrand, France, June 22nd - 24th 2015. e-ISBN: 978-2-35158-154-4.

[21] D. Lelievre, T. Colinart, P. Glouannec, Hygrothermal behavior of bio-based building materials including hysteresis effects: Experimental and numerical analyses. Energ. Buildings 84 (2014) 617–627. https://doi.org/10.1016/j.enbuild.2014.09.013.

[22] T. Colinart, D. Lelievre, P. Glouannec, Experimental and numerical analysis of the transient hygrothermal behavior of multilayered hemp concrete wall, Energ. Buildings 112 (2016) 1–11. https://doi.org/10.1016/j.enbuild.2015.11.027.

[23] T. Colinart, P. Glouannec, M. Bendouma, P. Chauvelon, Temperature dependence of sorption isotherm of hygroscopic building materials. Part 2: Influence on hygrothermal behavior of hemp concrete, Energ. Buildings 152 (2017) 42–51. https://doi.org/10.1016/j.enbuild.2017.07.016.

[24] M. Rahim, A.D. Tran Le, O. n Douzane, G. Promis, T. Langlet, Numerical investigation of the effect of non-isotherm sorption characteristics on hygrothermal behavior of two bio-based building walls, J. Build. Eng. 7 (2016) 263–272. https://doi.org/10.1016/j.jobe.2016.07.003.

[25] A. Fabbri, F. McGregor, Impact of the determination of the sorption-desorption curves on the prediction of the hemp concrete hygrothermal behaviour, Constr. Build. Mater. 157 (2017) 108–116. https://doi.org/10.1016/j.conbuildmat.2017.09.077.

[26] B. Seng, S. Lorente, C. Magniont, Scale analysis of heat and moisture transfer through bio-based materials — Application to hemp concrete, Energ. Buildings 155 (2017) 546–558. https://doi.org/10.1016/j.enbuild.2017.09.026.

[27] F. Collet, S. Pretot, V. Colson, C.R. Gamble, N. Reuge, C. Lanos, Hygric properties of materials used for ISOBIO wall solution for new buildings, in: 3rd International Conference on Bio-Based Building Materials, Belfast, UK, June 26th - 28th 2019. https://doi.org/10.26168/icbbm2019.50.

[28] M.Th. Van Genuchten, A closed-form equation for predicting the hydraulic conductivity of unsatured soils, Soil Sci. Soc. Am. J. 4 (1980) 892-898. https://doi.org/10.2136/sssaj1980.03615995004400050002x.

[29] F. Collet, S. Pretot, Thermal conductivity of hemp concretes: Variation with formulation, density and water content, Constr. Build. Mater. 65 (2014) 612–619. https://doi.org/10.1016/j.conbuildmat.2014.05.039.

[30] F. Collet, M. Bart, L. Serres, J. Miriel, Porous structure and water vapour sorption of hemp-based materials, Constr. Build. Mater. 22 (2008) 1271–1280. https://doi.org/10.1016/j.conbuildmat.2007.01.018.

[31] L.H. Mortensen, C. Rode, R. Peuhkuri, Effect of airflow velocity on moisture exchange at surfaces, BYG-DTU, Trondheim, October 26-28 2005. ISBN 0-415-41675-2.

[32] G. Talev, B.P. Jelle, E. Næss, A. Gustavsen, J.V. Thue, Measurement of the convective moisture transfer coefficient from porous building material surfaces applying a wind tunnel method, J. Build. Phys. 37(1) (2012) 103-121. https://doi.org/10.1177/1744259112459262.

Nomenclature

Latin symbols

Cp_0	Specific heat capacity at dry state ($J.kg^{-1}.K^{-1}$)
D_v	Vapor diffusivity in air ($m^2.s^{-1}$)
$D_{p,v}$	Vapor diffusivity in a porous medium ($m^2.s^{-1}$)
$D_{p,l}$	Liquid water diffusivity in a porous medium ($m^2.s^{-1}$)
h	Adjustment coefficient according to eq. (1)
h_m	Mass transfer coefficient ($kg.m^{-2}.Pa^{-1}.s^{-1}$)
k_0	Local kinetic constant defined in eq. (5) ($day^{-1}/(kg.m^{-3})$)
k_{01}	Local kinetic constant defined in eq. (9) ($day^{-1}/(kg.m^{-3})$)
k_{02}	Local kinetic constant defined in eq. (9) ($m.kg^{-3}$)
M_w	Water molar mass ($kg.mol^{-1}$)
P_{sat}	Saturation vapor pressure in air (Pa)
r	Correlation coefficient (-)
R	Gas constant ($J.mol^{-1}.K^{-1}$)
R_s	Sorption rate ($kg.m^{-3}.s^{-1}$)
RH	Ambient relative humidity or global relative humidity in a sample (-)
T	Temperature (K)
t	Time (s)
w	Local water content ($kg.m^{-3}$)
w_{eq}	Local equilibrium water content ($kg.m^{-3}$)
W	Global water content in a sample ($kg.m^{-3}$)
W_{eq}	Equilibrium water content in a sample ($kg.m^{-3}$)
W_{sat}	Maximum water content in a sample ($kg.m^{-3}$)

Greek symbols

β	Coefficient defined in eq. (8) (-)
δ_v	Vapor permeability of air ($kg.Pa^{-1}.m^{-1}.s^{-1}$)
$\delta_{v,p}$	Vapor permeability of a porous sample ($kg.Pa^{-1}.m^{-1}.s^{-1}$)
ε_0	Porosity (-)

η	Adjustment coefficient according to eq. (1)
λ	Thermal conductivity ($W.m^{-1}.K^{-1}$)
λ_0	Thermal conductivity at dry state ($W.m^{-1}.K^{-1}$)
λ_a	Thermal conductivity of air ($W.m^{-1}.K^{-1}$)
λ_s	Adjustment coefficient according to eq. (2)
λ_w	Thermal conductivity of water ($W.m^{-1}.K^{-1}$)
μ	Vapor diffusion resistance factor (-)
μ_0	Vapor diffusion resistance factor at dry state (-)
φ	Local relative humidity (-)
ρ_0	Density at dry state ($kg.m^{-3}$)

Acronyms (ISOBIO materials)

BCB	lime-hemp render from BCB™
BIO	Biofib Trio flexible insulation panel from CAVAC™
CAV	Rigid insulation panel from CAVAC™
CLA	Clay-hemp plaster from CLAYTEC™
CSB	Lignicell CSB™ panel
OSB3	Oriented Strand Board

Figures captions

Figure 1: ISOBIO multilayered reference wall

Figure 2: Isotherms of adsorption of CAV and CSB materials – Experimental data (symbols) and adjustments with the VG model (lines)

Figure 3: Kinetics of adsorption at the sample scale (150x150x45 mm^3) for CAV material – Measurements and simulations with local kinetics models (5) and (9)

Figure 4: MBV test (Nordtest project's protocol) – Smoothed curve of the ambient *RH*

Figure 5: Temporal evolution of relative water mass in the CAV sample – Measurements, TMC & TMCKIN simulations

Figure 6: Temporal evolution of relative water mass in the CSB sample – Measurements, TMC & TMCKIN simulations

Figure 7: Temporal evolution of relative water mass in the BCB sample – Measurements, TMC & TMCKIN simulations

Figure 8: Temporal evolution of relative water mass in the OSB3 sample – Measurements, TMC & TMCKIN simulations

Figure 9: CAV sample submitted to hygric cycles, results between t = 48 h and t = 72 h, local results from TMC & TMCKIN simulations at 2 mm and 2 cm depths

Figure 10: CAV sample – Water content profiles and relative water content distributions by slices of 1 cm compared to initial water content W_{eq}(50% *RH*) as a function of sample depth at t = 48 h (black) and t = 56 h (red) – TMC (a) & TMCKIN (b) simulations

Figure 11: General view of the bi-climatic room used for this study, monitoring system

Figure 12: *RH* and *T* measured at the wall surfaces during period 1, (a) and (b), period 2, (c) and (d), and period 3, (e) and (f)

Figure 13: Temporal evolution of *RH* at positions 1 (a), 2 (b) and 3 (c) – Period 1 – Measurements, TMC & TMCKIN simulations

Figure 14: Temporal evolution of *RH* at positions 1 (a), 2 (b) and 3 (c) – Period 2 – Measurements, TMC & TMCKIN simulations

Figure 15: Temporal evolution of *RH* at positions 1 (a), 2 (b) and 3 (c) – Period 3 – Measurements, TMC & TMCKIN simulations

Figure 16: Temporal evolution of *RH* at positions 2 – Period 3 – Measurements, TMC results +2%*RH* & TMCKIN results +2%*RH*

All Figures in color excepted Figures 1 and 4

2-column fitting images are required for Figures 3, 10, 12, 13, 14 and 15

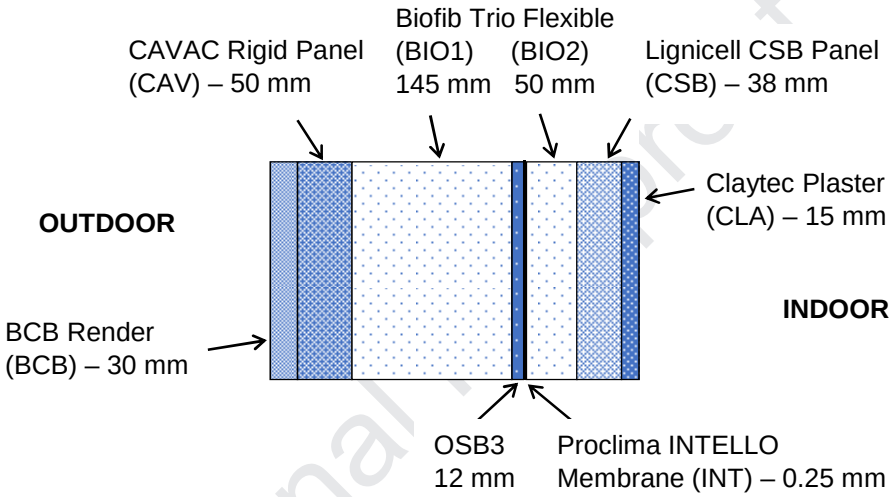
Biofib Trio Flexible
CAVAC Rigid Panel
(CAV) – 50 mm
(BIO1)
145 mm
(BIO2)
50 mm
Lignicell CSB Panel
(CSB) – 38 mm
Claytec Plaster
(CLA) – 15 mm
OUTDOOR
INDOOR
BCB Render
(BCB) – 30 mm
OSB3
12 mm
Proclima INTELLO
Membrane (INT) – 0.25 mm

Figure 1

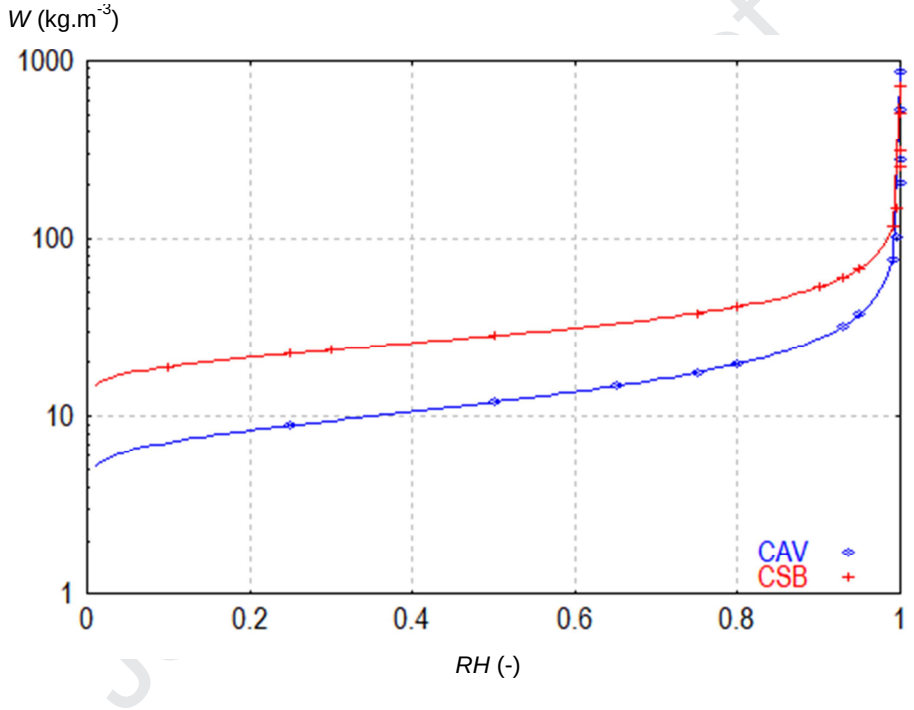

Figure 2

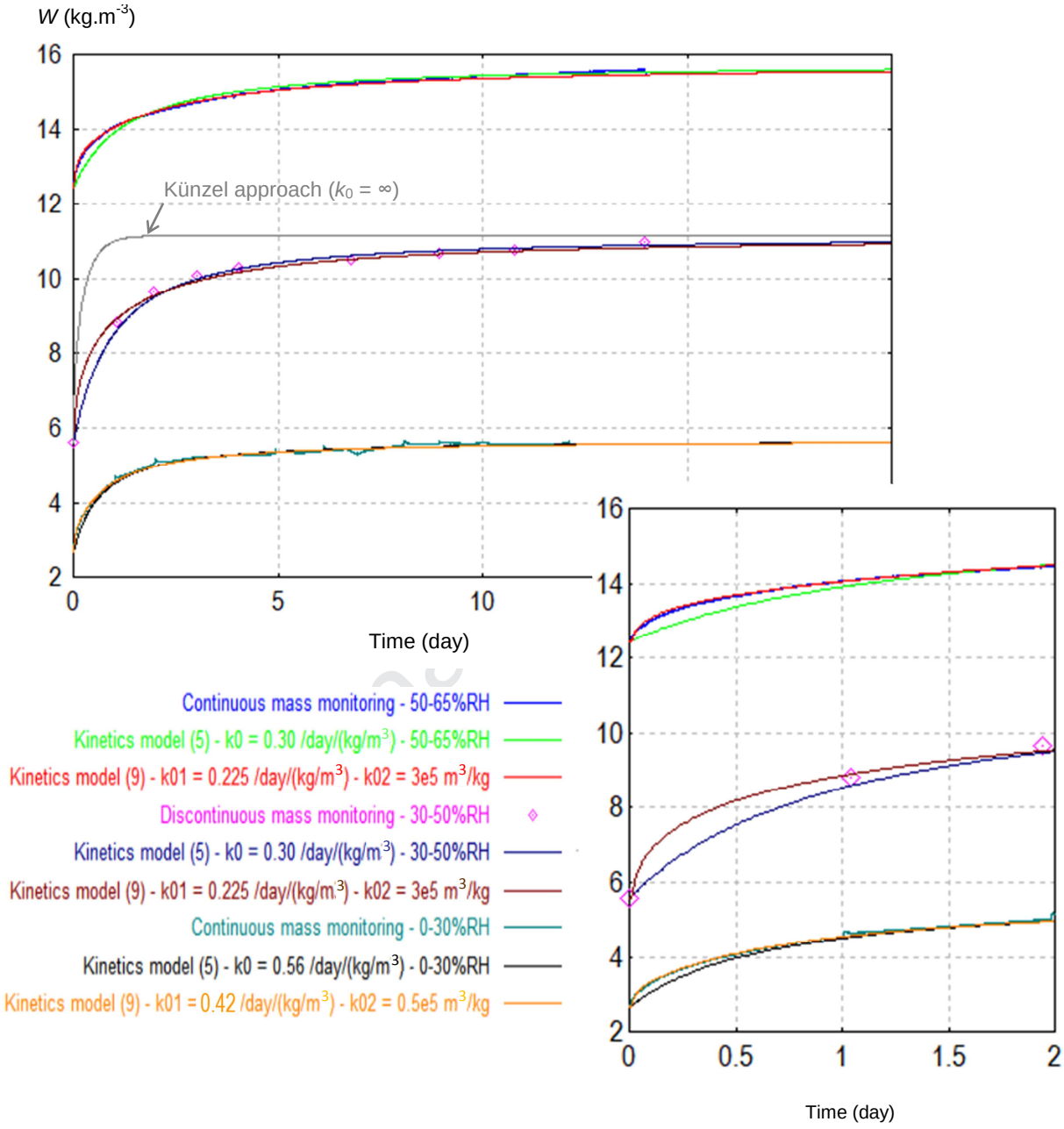
W (kg.m-3)
Künzel approach (k0 = ∞)
Time (day)
Continuous mass monitoring - 50-65%RH
Kinetics model (5) - k0 = 0.30 /day/(kg/m3) - 50-65%RH
Kinetics model (9) - k01 = 0.225 /day/(kg/m3) - k02 = 3e5 m3/kg
Discontinuous mass monitoring - 30-50%RH
Kinetics model (5) - k0 = 0.30 /day/(kg/m3) - 30-50%RH
Kinetics model (9) - k01 = 0.225 /day/(kg/m3) - k02 = 3e5 m3/kg
Continuous mass monitoring - 0-30%RH
Kinetics model (5) - k0 = 0.56 /day/(kg/m3) - 0-30%RH
Kinetics model (9) - k01 = 0.42 /day/(kg/m3) - k02 = 0.5e5 m3/kg
Time (day)

Figure 3

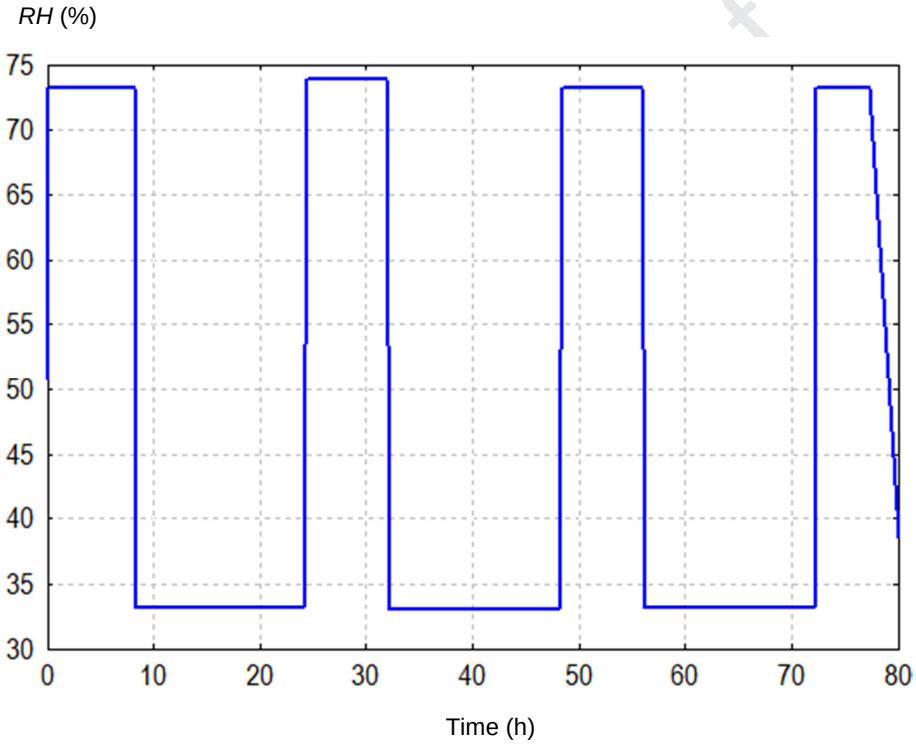

Figure 4

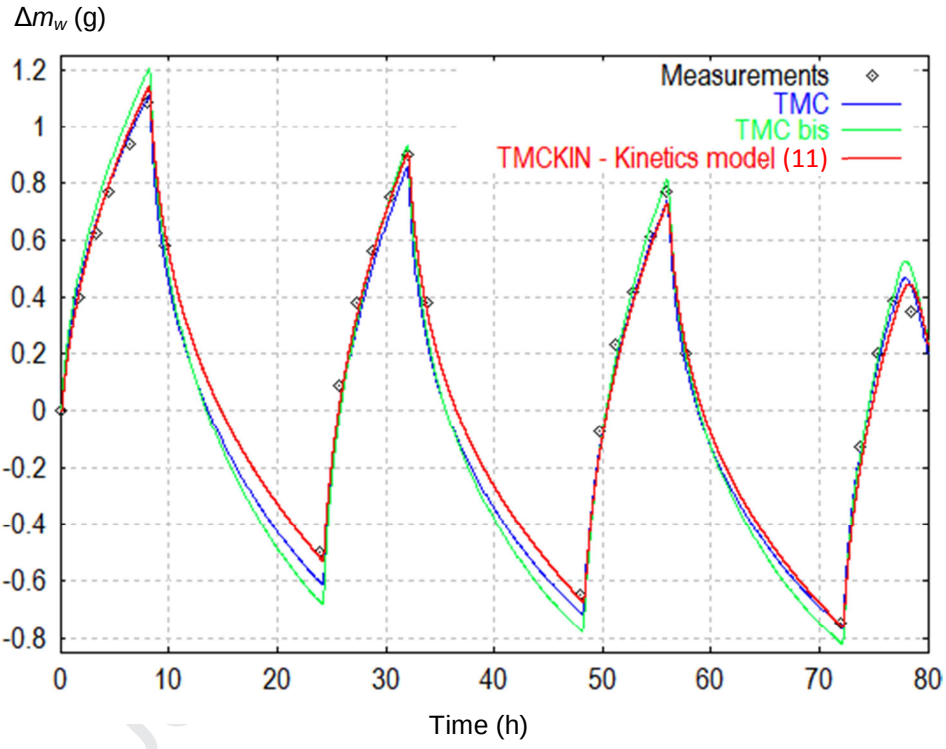
Δm_w (g)
1.2
1
0.8
0.6
0.4
0.2
0
-0.2
-0.4
-0.6
-0.8
0
10
20
30
40
50
60
70
80
Time (h)
Measurements
TMC
TMC bis
TMCKIN - Kinetics model (11)

Figure 5

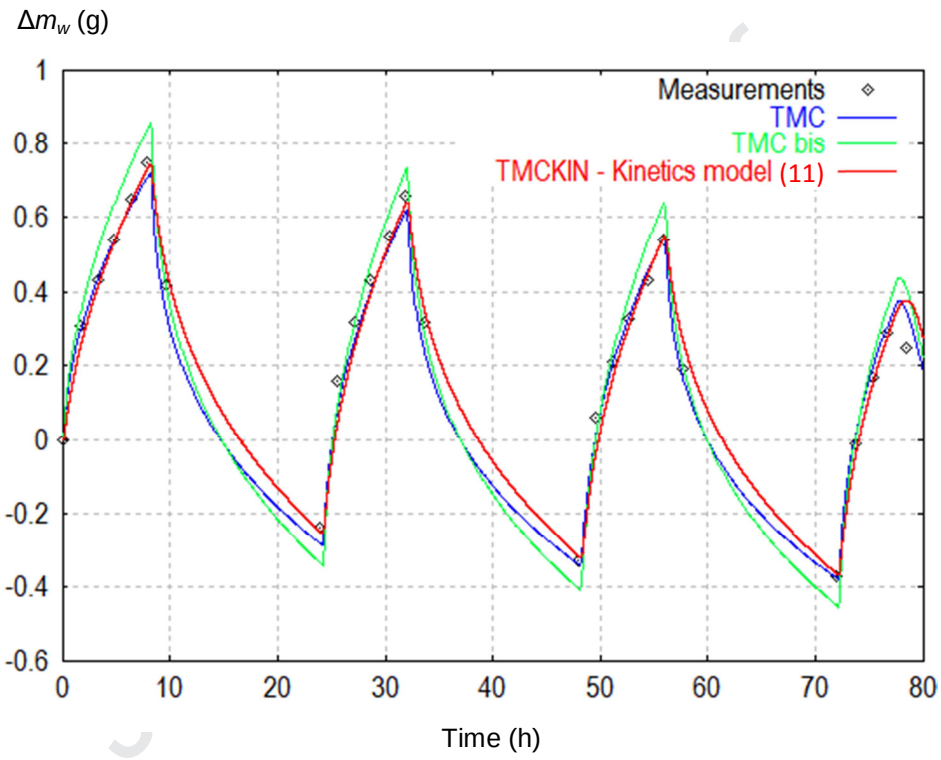
Δm_w (g)
1
0.8
0.6
0.4
0.2
0
-0.2
-0.4
-0.6
0
10
20
30
40
50
60
70
80
Time (h)
Measurements
TMC
TMC bis
TMCKIN - Kinetics model (11)

Figure 6

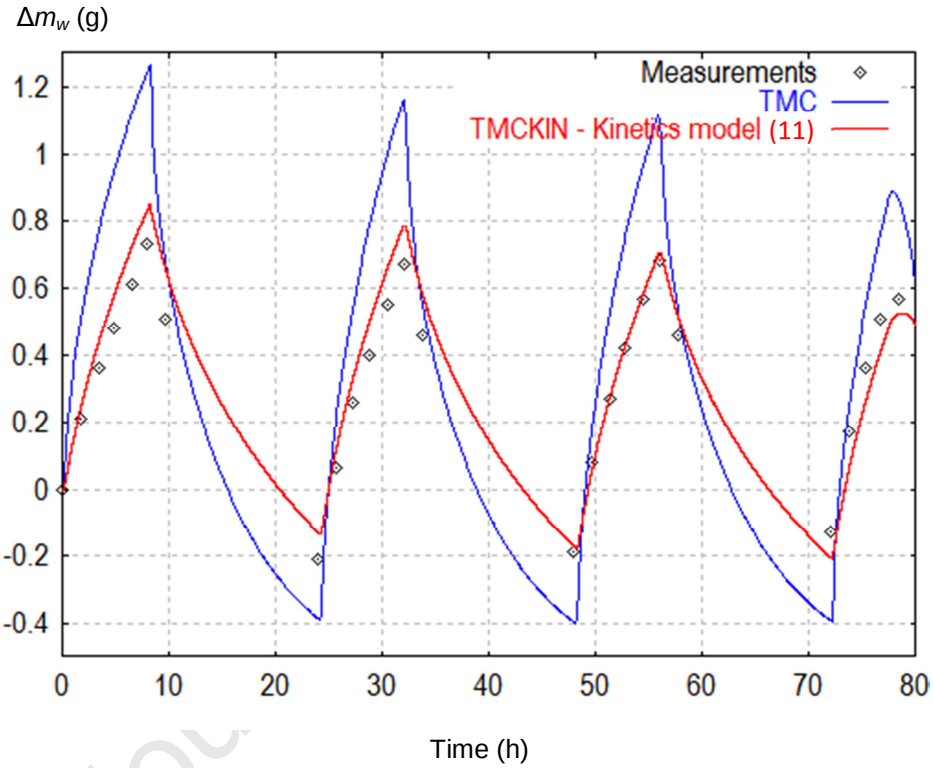
Δm_w (g)
Measurements
TMC
TMCKIN - Kinetics model (11)
1.2
1
0.8
0.6
0.4
0.2
0
-0.2
-0.4
0
10
20
30
40
50
60
70
80
Time (h)

Figure 7

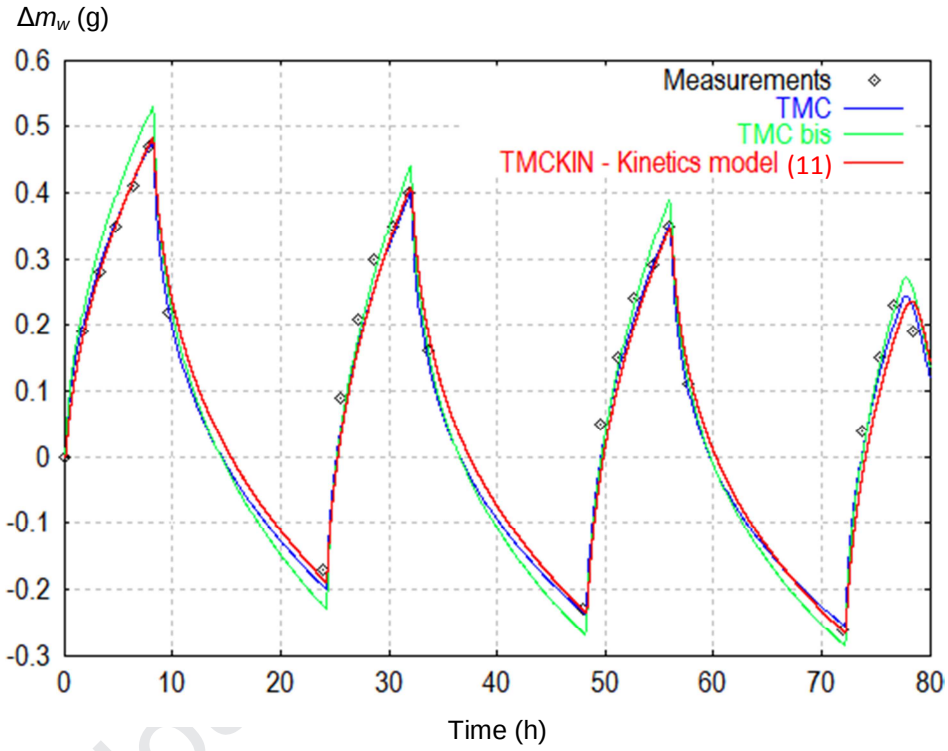
Δm_w (g)
0.6
0.5
0.4
0.3
0.2
0.1
0
-0.1
-0.2
-0.3
0
10
20
30
40
50
60
70
80
Time (h)
Measurements
TMC
TMC bis
TMCKIN - Kinetics model (11)

Figure 8

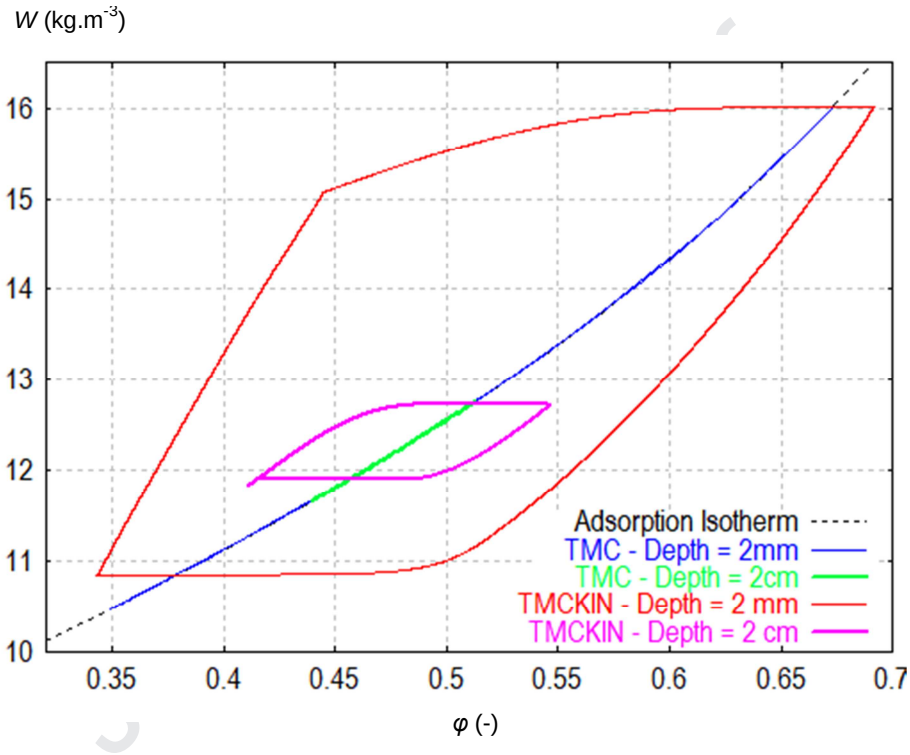
W (kg.m-3)
16
15
14
13
12
11
10
0.35
0.4
0.45
0.5
0.55
0.6
0.65
0.7
φ (-)
Adsorption Isotherm
TMC - Depth = 2mm
TMC - Depth = 2cm
TMCKIN - Depth = 2 mm
TMCKIN - Depth = 2 cm

Figure 9

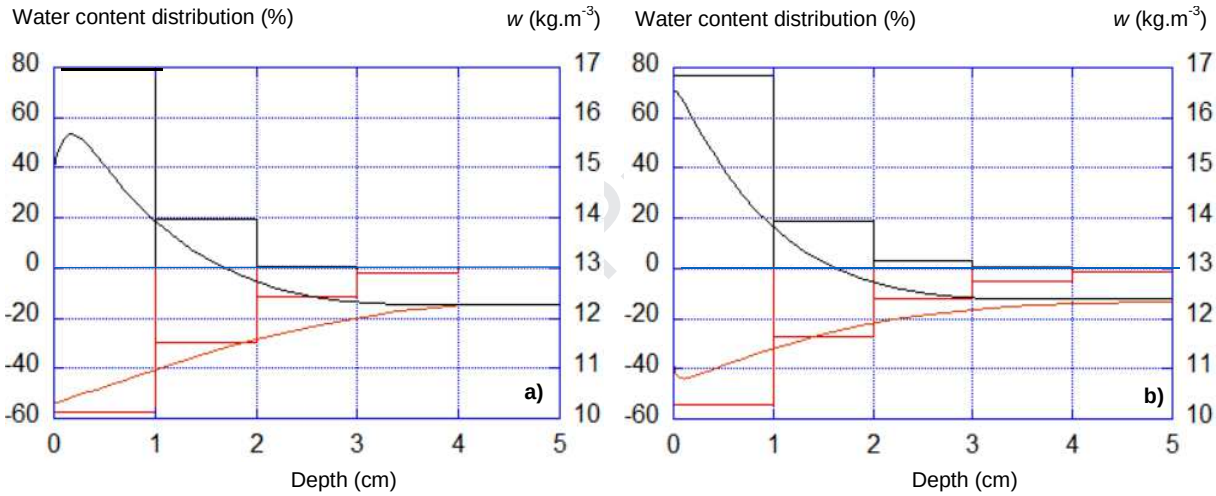
Water content distribution (%)
w (kg.m-3)
80
60
40
20
0
-20
-40
-60
17
16
15
14
13
12
11
10
0
1
2
3
4
5
Depth (cm)
a)
Water content distribution (%)
w (kg.m-3)
Depth (cm)
b)

Figure 10

Figure 11

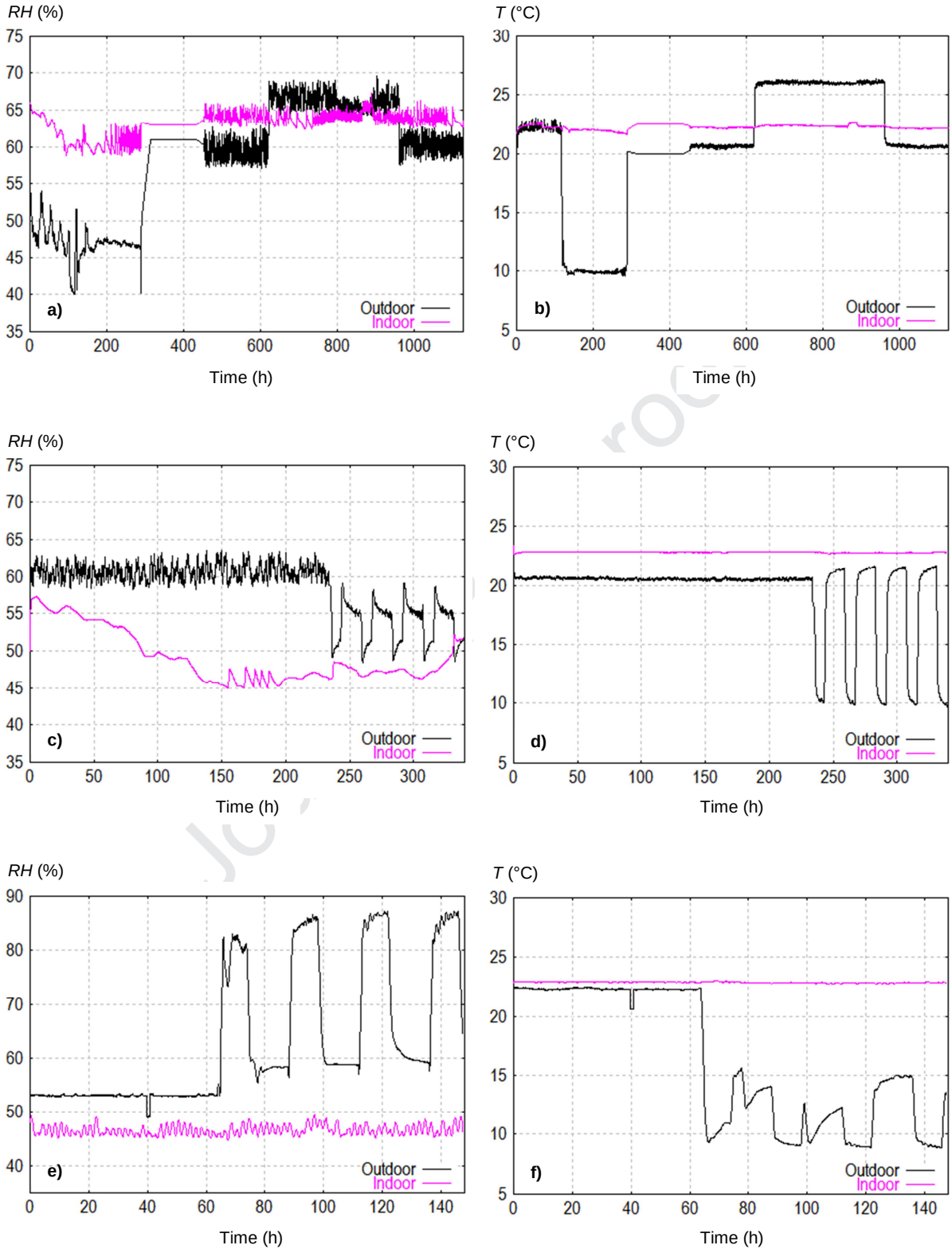

Figure 12

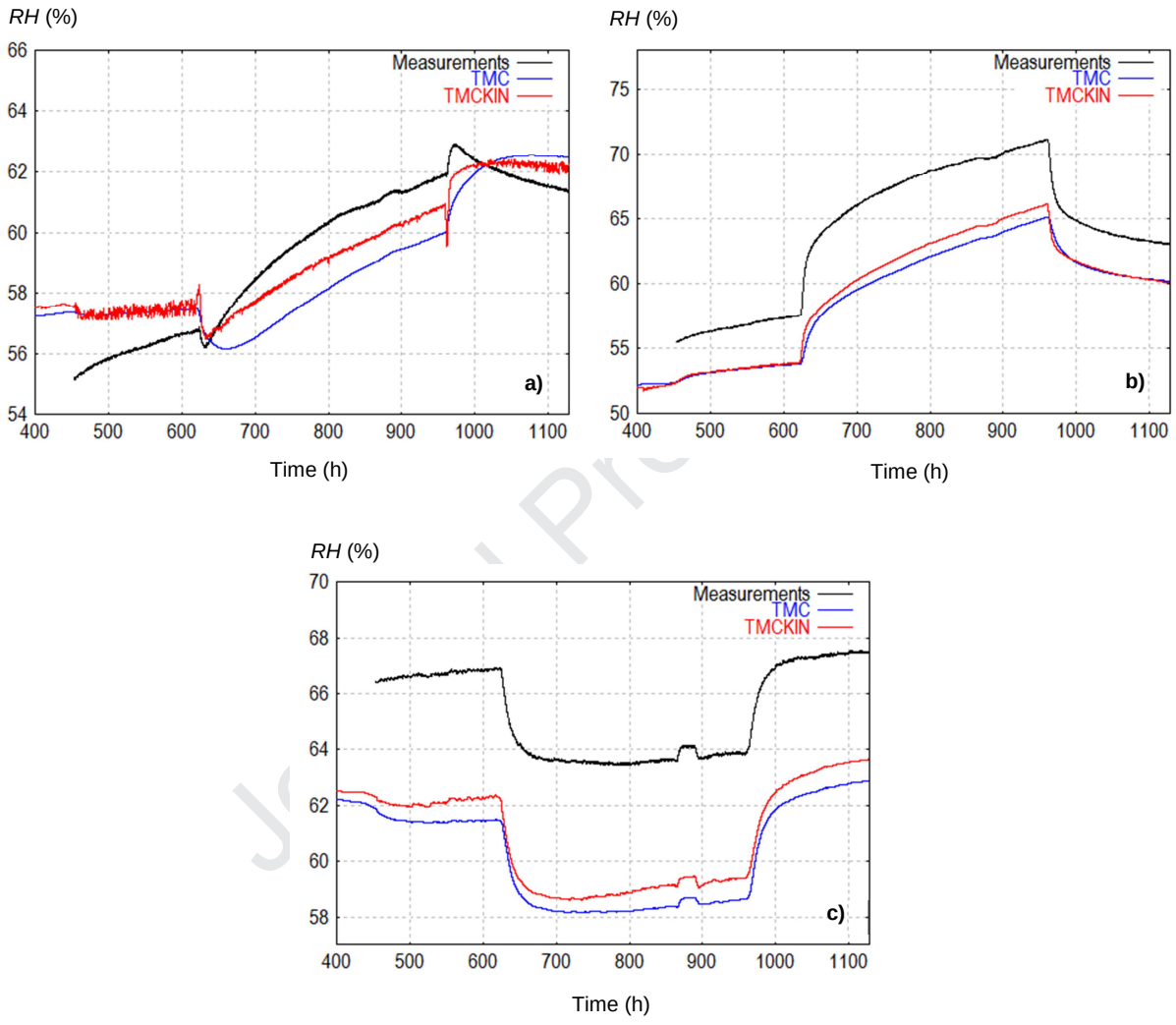
RH (%)
Measurements
TMC
TMCKIN
a)
Time (h)
RH (%)
Measurements
TMC
TMCKIN
b)
Time (h)
RH (%)
Measurements
TMC
TMCKIN
c)
Time (h)

Figure 13

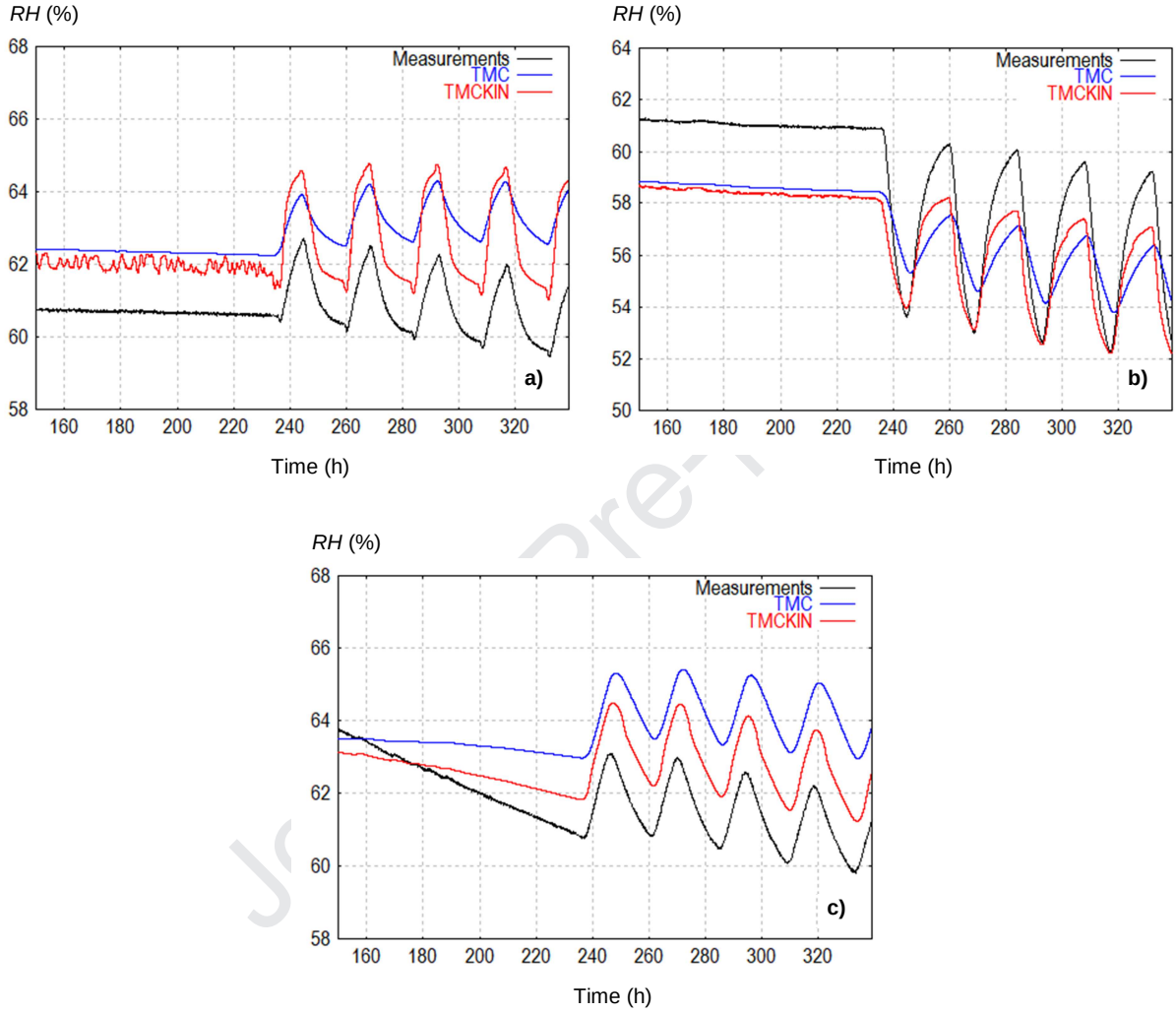

Figure 14

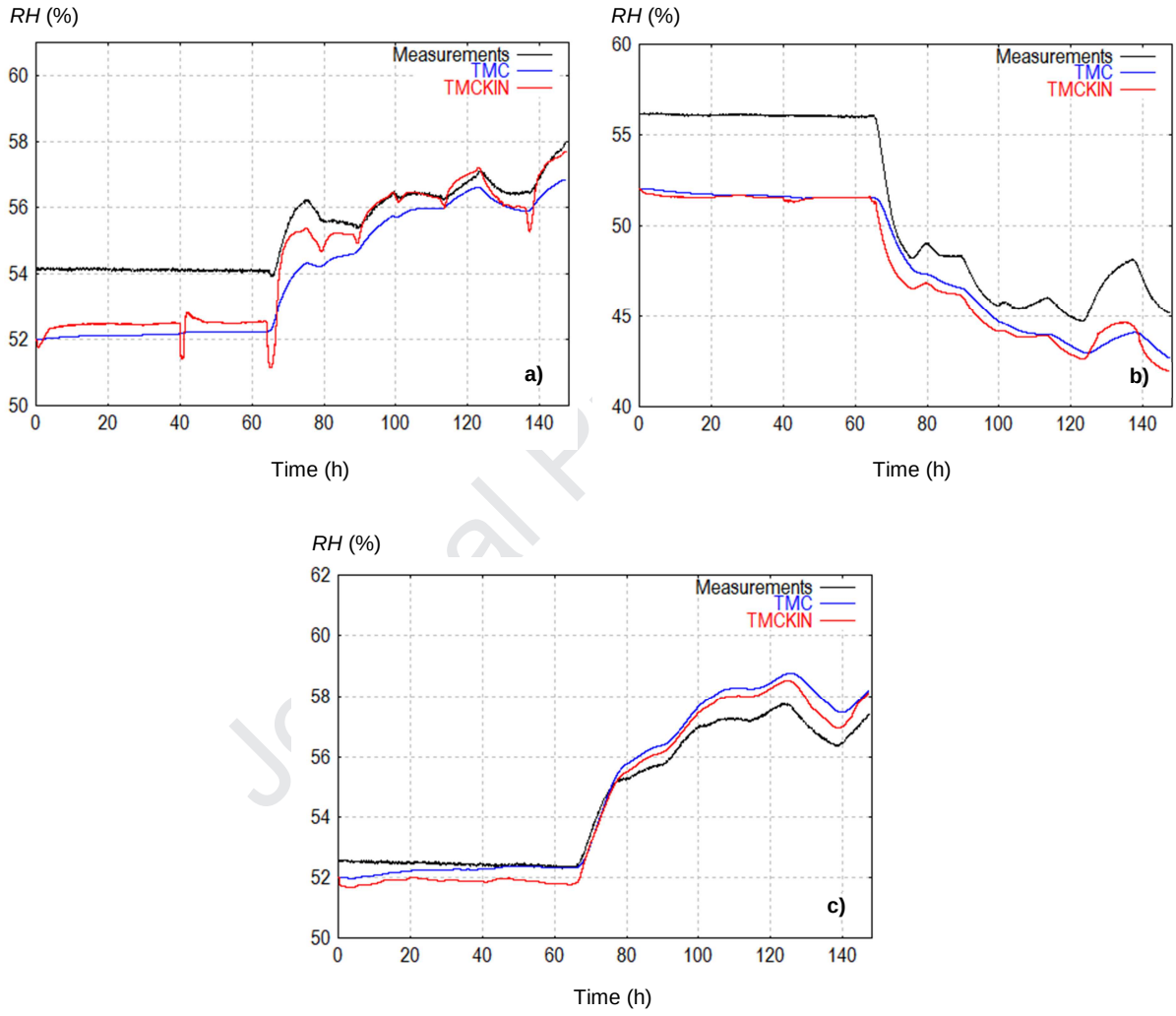
RH (%)
Measurements
TMC
TMCKIN
a)
Time (h)
RH (%)
Measurements
TMC
TMCKIN
b)
Time (h)
RH (%)
Measurements
TMC
TMCKIN
c)
Time (h)

Figure 15

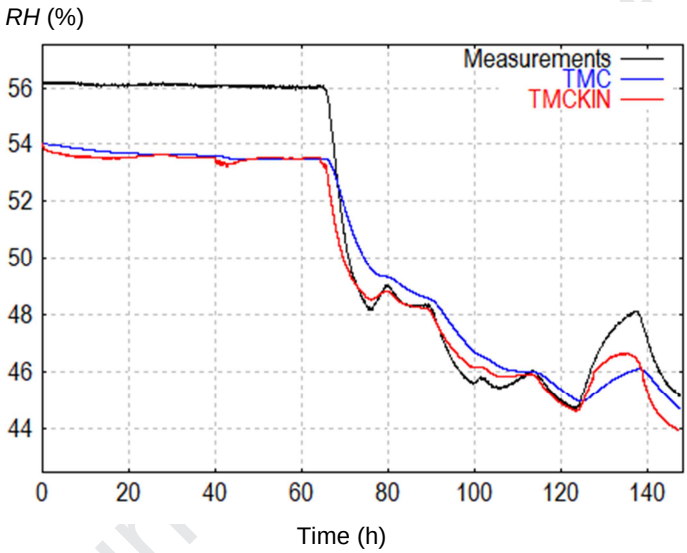
RH (%)
Measurements
TMC
TMCKIN
56
54
52
50
48
46
44
0
20
40
60
80
100
120
140
Time (h)

Figure 16

Article highlights

- Improvement of the local kinetics of sorption model

- Comparisons of measurements / simulations of Moisture Buffer Value tests according to the Nordtest project's protocol

- One of the first comparisons of measurements / simulations of a fully bio-based porous wall in the controlled environment of a bi-climatic chamber

Declaration of interest:

None